Modal stability of inclined cables subjected to harmonic excitation

A. Gonzalez-Buelga, S.A. Neild*, D.J. Wagg and J.H.G. Macdonald

University of Bristol, Queens Building, University Walk
Bristol BS8 1TR, U.K.

October 15, 2007

Abstract

In this paper the out-of-plane stability of cables subjected to in-plane dynamic loading is investigated. We compute stability boundaries for the out-of plane modes using rescaling and averaging methods. Our study focuses on the 2:1internal resonance phenomena, that occurs when the external excitation frequency is twice the first out-of-plane natural frequency of the cable. An analytical model is developed in order to study the stability regions in parameter space. In this model we include nonlinear modal coupling effects which have thus far been ommitted from previous models of inclined cables. Our study reflects the importance of such effects. Unstable parameter regions are defined for the selected cable configurations to highlight the effects of the nondimensional cable parameters. The validity of the proposed stability model was tested experimentally using a small scale cable actuator rig. A comparison between experimental and analytical results is presented in which very good agreement with model predictions were obtained.

Key words: Internal resonance, Stability, Mathieu equation, cable dynamics, nonlinear.

1 Introduction

Cable-supported structures such as cable-stay bridges can exhibit undesirable dynamic properties especially when the structure is flexible and lightly damped. Cable dynamics are strongly nonlinear, with internal coupling between modes and parametric coupling with external effects, such as the deck dynamics

*Author for correspondance:simon.neild@bristol.ac.uk, Tel: +44 (117) 928 9730, Fax : +44 (117) 929 4423

in the case of a cable-stay bridge. These nonlinear effects can produce complex behaviour resulting in large amplitude cable vibrations, see for example the review by Nayfeh and Pai [1]. Internal resonance can occur at specific ratios of excitation frequency to cable natural frequency, the most significant of which occurs at the 2:1 ratio, at which small excitation amplitudes at the cable anchorage can result in very large cable vibrations [2]. These vibrations can occur in-plane (defined as the plane in which the cable sags statically) or out-of-plane even if the anchorage excitation is limited to just the in-plane direction, as would typically be the case when a cable-stay bridge cable is excited by deck motion.

It has been shown that, provided sag is small, the second in-plane and out-of-plane cable natural frequencies are at twice the first out-of-plane natural frequency [3]. If the support motion is close to 2:1 resonance of the first out-of-plane mode it will directly excite the second in-plane mode. Due to cable non-linearity, the motion of the second in-plane mode and the external excitation may, if the excitation is of sufficient amplitude, induce internal resonance of either the first or the second out-of-plane cable modes or both modes. This paper concentrates of determining the level of vertical excitation of the lower cable support required for the onset of an internally excited out-of-plane response. We refer to the onset of an out-of-plane response as the instability point of the semi-trivial solution – the solution where only the second in-plane mode is excited.

Modal stability studies of cable dynamics that consider internal resonance are usually based on the Mathieu or Hill equation [4, 5]. For example [2] considered response in a single cable mode. The study presented in [6] included more than one mode of vibration but without modal coupling and so the problem reduces to uncoupled Mathieu equations. The simulation studies reported by [7–9] include both in-plane and out-of-plane modes of horizontal cables and include some nonlinear interactions between these modes, however explicit stability regions are not calculated. We use the modal model to compute the instability boundary for a range of excitation frequencies close to 2:1 resonance. For a specific excitation frequency, the point of instability is found by considering the local stability of the out-of-plane modes as the excitation amplitude increases. The point at which either out-of-plane modes has non-zero response indicates the onset of oscillations for that mode and hence the semi-trivial solution is no longer stable.

The experimental setup consists of a cable attached to an electro-mechanic actuator, such that the lower anchor point can be excited vertically, and data is acquired with a high speed vision system [10]. The points of instability of the semi-trivial solution are detected in the experiment, by looking for the onset of oscillations in the out-of-plane modes. We note that the first in-plane mode is less susceptible to internal resonance when the excitation is at approximately twice the first out-of-plane frequency as the modal frequency is higher than the first out-of-plane frequency due to the cable sag [3]. However as

the excitation frequency increases this mode may also be excited. Consideration of this mode is beyond the scope of the present study but the frequencies at which this mode is excited are highlighted in the experimental results.

In section 2 a theoretical study of the stability of the semi-trivial solution is presented. The accuracy of the theoretical results are assessed in section 3 by testing a small-scale cable both in simulation and experimentally. A parametric study of the stability boundary is presented in section 4 and conclusions are drawn in section 5.

2 Theoretical study

Firstly we present a modal model of the cable dynamics [11]. In the system considered here, when the excitation at close to twice the first out-of-plane natural frequency, the second in-plane mode is excited directly. In addition to this the first and second out-of-plane modes may be excited parametrically or via non-linear modal coupling. We therefore reduce the model to these three modes of interest. At higher excitation frequencies the first in-plane mode may also be excited parametrically but as noted in the introduction this is beyond the scope of the present study. Considering the three modes of interest, the second step in the analysis is to scale the equations and introduce detuning in the excitation frequency to allow a study close to 2:1 resonance. We perform first-order averaging to derive first-order differential equations of the response amplitudes for the sine and cosine components of the three modes. In the third step of the analysis we use these equations to assess the local stability at the zero amplitude point for the two out-of-plane modes in the presence of the external excitation and in-plane motion. For either of the out-of-plane modes, local instability at the zero amplitude point will result in a response in that mode and hence mark the stability boundary of the semi-trivial solution. Finally, we consider the amplitude of response of the second in-plane mode just below the stability boundary of the semi-trivial solution and use this to derive a relationship between the excitation amplitude and frequency detuning parameter at the semi-trivial solution stability boundary. These stability boundaries can be plotted in parameter space to indicate regions of stability and instability for each mode similar to an Arnold tongues in a single degree of freedom Mathieu equation [REF?].

2.1 Step 1 - Equations of motion

There have been many presentations of the equations of motion for cables [1]. In this paper we adopt the modal equations derived by Warnitchai *et al.* [11]. Their derivation includes the effect of support motion at both ends of the cable and accounts for quadratic and cubic nonlinearities. The cable is

supported at end points a and b and the direction of the chord line from a to b is defined as x, see figure 1. The cable equilibrium sag position and the chord line both lie in the $x-z$ plane, therefore z represents in-plane motion and y represents out-of-plane motion. The angle between the chord line and the horizontal is given as θ corresponds to the angle of inclination. Following [11], the modal representation of the out-of-plane cable motion may be expressed as [11]

$$\begin{aligned} m_{yn}\left(\ddot{y}_n + 2\xi_{yn}\omega_{yn}\dot{y}_n + \omega_{yn}^2 y_n\right) + \sum_k \nu_{nk} y_n \left(y_k^2 + z_k^2\right) + \sum_k 2\beta_{nk} y_n z_k + \\ +2\eta_n\left(u_b - u_a\right) y_n + \zeta_n\left(\ddot{v}_a + (-1)^{n+1}\ddot{v}_b\right) = F_{yn} \end{aligned} \tag{1}$$

and the in-plane cable motion as

$$\begin{aligned} m_{zn}\left(\ddot{z}_n + 2\xi_{zn}\omega_{zn}\dot{z}_n + \omega_{zn}^2 z_n\right) + \sum_k \nu_{nk} z_n \left(y_k^2 + z_k^2\right) + \sum_k 2\beta_{nk} z_n z_k + \sum_k \beta_{kn}\left(y_k^2 + z_k^2\right) + \\ +2\eta_n\left(u_b - u_a\right) z_n + \zeta_n\left(\ddot{w}_a + (-1)^{n+1}\ddot{w}_b\right) - \alpha_n\left(\ddot{u}_b - \ddot{u}_a\right) = F_{zn} \end{aligned} \tag{2}$$

where y_n and z_n are the out-of-plane and in-plane generalised displacement of the cable in the n^{th} mode respectively; subscripts a and b denote the top and bottom anchorage points respectively; $m_{yn} = m_{zn} = m$ is the modal mass ($m = \rho AL/2$); L is the cable length; σ_s is the cable static stress; λ^2 is Irvine's parameter [REF], A is the cross section area, ρ is the density and E is the Young's Modulus. The equivalent modulus of the cable E_q, the distributed weight perpendicular to the cable cord γ, and the parameters k_n, ν_{nk}, β_{nk}, η_n, α_n, λ, and F_{yn} and F_{zn} which represent external cable loading in the y and z direction respectively are given by:

$$\begin{aligned} E_q &= \frac{1}{1+\frac{\lambda^2}{12}}E & \gamma &= \rho g cos\theta & \lambda &= \sqrt{\frac{E}{\sigma_s}}\frac{\gamma L}{\sigma_s} \\ \nu_{nk} &= \frac{EA\pi^4 n^2 k^2}{8L^3} & \beta_{nk} &= \frac{EA\pi\gamma n^2}{4L\sigma_s}\left(\frac{1+(-1)^{k+1}}{k}\right) & \eta_n &= \frac{E_q A\pi^2 n^2}{4L^2} \\ \zeta_n &= \frac{2m}{n\pi} & \alpha_n &= \frac{2m\gamma L E_q}{n^3\pi^3\sigma_s^2}\left(1+(-1)^{n+1}\right) & F_{yn} &= \int_0^L YA\phi_n \mathrm{d}x \\ & & & & F_{zn} &= \int_0^L ZA\psi_n \mathrm{d}x \end{aligned} \tag{3}$$

where ϕ_n and ψ_n are the out-of-plane and in-plane mode shapes. Finally, the out-of-plane and in-plane natural frequencies, ω_{yn} and ω_{zn} respectively, are given by

$$\omega_{yn} = \frac{n\pi}{L}\sqrt{\frac{\sigma_s}{\rho}} \quad , \quad \omega_{zn} = \frac{n\pi}{L}\sqrt{\frac{\sigma_s}{\rho}(1+k_n)} \tag{4}$$

Note that these equations assume that the sag and end displacements are small. Also it is assumed that damping can be modelled as viscous with modal damping ratios ξ_{zn} and ξ_{yn}. See Warnitchai *et al.* [11] for details of the derivation.

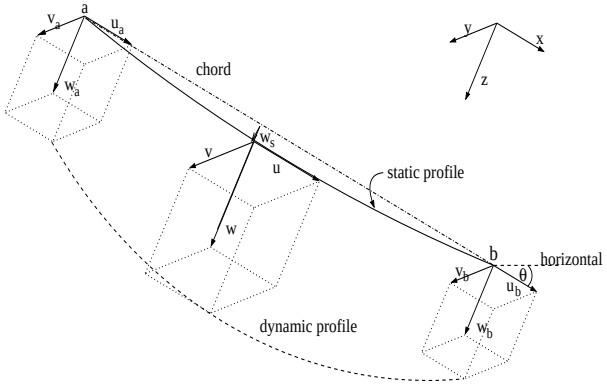

Figure 1: Definition of cable coordinate system [11]

2.2 Step 2 - Scaling and Averaging

The cable is excited vertically at the bottom anchorage (point b) with amplitude Δ and angular frequency Ω. In this case the end conditions are $u_a = v_a = w_a = 0$, $u_b = \delta \sin\theta$, $w_b = \delta \cos\theta$ and $v_b = 0$, where $\delta = \Delta \cos(\Omega t)$ is the vertical displacement applied by the actuator. No external forces are applied along the length of the cable.

In the simulation and experimental study presented in the next section the sag was such that $\omega_{y1} = 0.93\omega_{z1}$; the first out and in-plane modes are therefore sufficiently separated in frequency. The remaining modal frequencies have the relationships $\omega_{z2} = \omega_{y2} = 2\omega_{y1}$; we denote $\omega_2 = \omega_{z2} = \omega_{y2}$ and $\omega_1 = \omega_{y1}$. From equations (1) and (2), we can rewrite the modal equations of motion for the three modes being considered (assuming negligible response in other modes in the frequency range considered) as

$$\begin{aligned}
\ddot{y}_1 + 2\xi_{y1}\omega_1\dot{y}_1 + \omega_1^2 y_1 + W_{11}y_1^3 + W_{12}y_1\left(y_2^2 + z_2^2\right) + N_1\delta y_1 &= 0 \\
\ddot{y}_2 + 2\xi_{y2}\omega_2\dot{y}_2 + \omega_2^2 y_2 + W_{21}y_2y_1^2 + W_{22}y_2\left(y_2^2 + z_2^2\right) + N_2\delta y_2 &= 0 \\
\ddot{z}_2 + 2\xi_{z2}\omega_2\dot{z}_2 + \omega_2^2 z_2 + W_{21}z_2y_1^2 + W_{22}z_2\left(y_2^2 + z_2^2\right) + N_2\delta z_2 &= B\ddot{\delta}
\end{aligned} \tag{5}$$

where $W_{nk} = \nu_{nk}/m$, $N_n = 2\eta_n \sin\theta/m$ and $B = \zeta_2 \cos\theta/m$. This is a set of nonlinear Mathieu equations which we can examine via scaling and averaging.

Introducing the small parameter ϵ, we scale the equations such that they are in the standard Lagrange form, see [12] [13]:

$$\ddot{x} + \omega_n^2 x = \epsilon f(\dot{x}, x, t) \tag{6}$$

to reflect the fact that the response is dominated by the linear undamped response (a discussion of scaling is given in Bakri *et al* [14]). The following transforms are made $\xi_{y1} \rightarrow \epsilon\xi_{y1}$, $\xi_{y2} \rightarrow \epsilon\xi_{y2}$,$\xi_{z2} \rightarrow \epsilon\xi_{z2}$,

$(y_i, z_i) \rightarrow \epsilon^{1/2}(y_i, z_i)$, $B \rightarrow \epsilon^{1/2}B$ and $\delta \rightarrow \epsilon\delta$; giving

$$\begin{aligned}
\ddot{y}_1 + \omega_1^2 y_1 + \epsilon\left(2\xi_{y1}\omega_1\dot{y}_1 + N_1\delta y_1 + W_{11}y_1^3 + W_{12}y_1\left[y_2^2 + z_2^2\right]\right) = 0 \\
\ddot{y}_2 + \omega_2^2 y_2 + \epsilon\left(2\xi_{y2}\omega_2\dot{y}_2 + N_2\delta y_2 + W_{21}y_2y_1^2 + W_{22}y_2\left[y_2^2 + z_2^2\right]\right) = 0 \\
\ddot{z}_2 + \omega_2^2 z_2 + \epsilon\left(2\xi_{z2}\omega_2\dot{z}_2 + N_2\delta z_2 + W_{21}z_2y_1^2 + W_{22}z_2\left[y_2^2 + z_2^2\right]\right) = \epsilon B\ddot{\delta}
\end{aligned} \tag{7}$$

The forcing frequency is close to twice the first out-of-plane natural frequency, therefore we write $\Omega = 2\omega_1(1+\mu)$ and then scale $\mu \rightarrow \epsilon\mu$ such that $\Omega = 2\omega_1(1+\epsilon\mu)$ in the scaled domain. Using this, taking into account that $\omega_2 = 2\omega_1$ and applying the time transform $\tau = (1+\epsilon\mu)t$, we can write

$$\begin{aligned}
y_1^{''} + \omega_1^2 y_1 + \epsilon\left(2\xi_{y1}\omega_1 y_1^{'} + N_1\delta y_1 - 2\mu\omega_1^2 y_1 + W_{11}y_1^3 + W_{12}y_1\left[y_2^2 + z_2^2\right]\right) = \mathcal{O}(\epsilon^2) \\
y_2^{''} + \omega_2^2 y_2 + \epsilon\left(2\xi_{y2}\omega_2 y_2^{'} + N_2\delta y_2 - 2\mu\omega_2^2 y_2 + W_{21}y_2y_1^2 + W_{22}y_2\left[y_2^2 + z_2^2\right]\right) = \mathcal{O}(\epsilon^2) \\
z_2^{''} + \omega_2^2 z_2 + \epsilon\left(2\xi_{z2}\omega_2 z_2^{'} + N_2\delta z_2 - 2\mu\omega_2^2 z_2 + W_{21}z_2y_1^2 + W_{22}z_2\left[y_2^2 + z_2^2\right] - B\delta^{''}\right) = \mathcal{O}(\epsilon^2)
\end{aligned} \tag{8}$$

where $\{\}^{'}$ represents the derivative with respect to τ and we assume the higher order terms with respect to ϵ are negligible.

We introduce the notation $\{x_{11},\ x_{22},\ x_{32}\} = \{y_1,\ y_2,\ z_2\}$ where the second subscript in x_{ij} represents whether the variable relates to a first or second mode. We also introduce the shorthand version for the equations in 8

$$x_{ij}^{''} + \omega_j^2 x_{ij} = \epsilon X_i \quad \text{for} \quad \{i,j\} = \{1,1\},\{2,2\},\{3,2\} \tag{9}$$

The equations are now in a form which can be averaged (see for example [12–14]). We apply transformations to y_1, y_2 and z_2 in the form

$$x_{ij} = x_{ijc}\cos(\omega_j\tau) + x_{ijs}\sin(\omega_j\tau) \tag{10}$$

$$x_{ij}^{'} = -\omega_j x_{ijc}\sin(\omega_j\tau) + \omega_j x_{ijs}\cos(\omega_j\tau) \tag{11}$$

Applying these transforms to equation (9) and applying the condition that the derivative of the right hand side of equation (10) must equal the right hand side of equation (11) for all three modes gives:

$$x_{ijc}^{'} = -\tfrac{\epsilon}{\omega_j}\sin(\omega_j\tau)X_i \quad , \quad x_{ijs}^{'} = \tfrac{\epsilon}{\omega_j}\cos(\omega_j\tau)X_i \tag{12}$$

where we note that the transforms in equations (10) and (11) must also be applied within the functions X_i. From inspection of the equations in 12, it can be seen that the derivative terms of x_{ijc} and x_{ijs} are small and so over a short timespan x_{ijc} and x_{ijs} may be treated as constant [13]. We can therefore

average equations (12) over an oscillation at frequency ω_1, treating the x_{ijc} and x_{ijs} terms within X_i as constant over the oscillation (taking the values x_{ijca} and x_{ijsa}, where subscript a indicates that they are approximate averaged values). During the averaging process many of the terms within X_i are averaged out indicating that although these terms affect the oscillation amplitude of x_{ij} they do not affect the underlying amplitude trajectory of x_{ij}. Applying the technique gives the following equations for the averaged parameters

$$\begin{aligned}
y_{1ca}^{'} &= -\tfrac{\epsilon}{\omega_1}\left(\xi_{y1}\omega_1^2 y_{1ca} + [\mu\omega_1^2 - \tfrac{N_1}{4}\Delta]y_{1sa} - \tfrac{3}{8}W_{11}y_{1sa}Y_{1a}^2 - \tfrac{1}{4}W_{12}y_{1sa}[Y_{2a}^2 + Z_{2a}^2]\right)\\
y_{1sa}^{'} &= \tfrac{\epsilon}{\omega_1}\left([\mu\omega_1^2 - \tfrac{N_1}{4}\Delta]y_{1ca} - \xi_{y1}\omega_1^2 y_{1sa} - \tfrac{3}{8}W_{11}y_{1ca}Y_{1a}^2 - \tfrac{1}{4}W_{12}y_{1ca}[Y_{2a}^2 + Z_{2a}^2]\right)\\
y_{2ca}^{'} &= -\tfrac{\epsilon}{\omega_2}\left(\xi_{y2}\omega_2^2 y_{2ca} + \mu\omega_2^2 y_{2sa} - \tfrac{1}{4}W_{21}y_{2sa}Y_{1a}^2 - \tfrac{1}{8}W_{22}y_{2sa}[3Y_{2a}^2 + Z_{2a}^2] - \tfrac{1}{4}W_{22}z_{2sa}C_{2a}\right)\\
y_{2sa}^{'} &= \tfrac{\epsilon}{\omega_2}\left(\mu\omega_2^2 y_{2ca} - \xi_{y2}\omega_2^2 y_{2sa} - \tfrac{1}{4}W_{21}y_{2ca}Y_{1a}^2 - \tfrac{1}{8}W_{22}y_{2ca}[3Y_{2a}^2 + Z_{2a}^2] - \tfrac{1}{4}W_{22}z_{2ca}C_{2a}\right)\\
z_{2ca}^{'} &= -\tfrac{\epsilon}{\omega_2}\left(\xi_{z2}\omega_2^2 z_{2ca} + \mu\omega_2^2 z_{2sa} - \tfrac{1}{4}W_{21}z_{2sa}Y_{1a}^2 - \tfrac{1}{8}W_{22}z_{2sa}[3Z_{2a}^2 + Y_{2a}^2] - \tfrac{1}{4}W_{22}y_{2sa}C_{2a}\right)\\
z_{2sa}^{'} &= \tfrac{\epsilon}{\omega_2}\left(\mu\omega_2^2 z_{2ca} - \xi_{z2}\omega_2^2 z_{2sa} - \tfrac{1}{4}W_{21}z_{2ca}Y_{1a}^2 - \tfrac{1}{8}W_{22}z_{2ca}[3Z_{2a}^2 + Y_{2a}^2] - \tfrac{1}{4}W_{22}y_{2ca}C_{2a} - \tfrac{1}{2}B\Delta\omega_2^2\right)
\end{aligned} \tag{13}$$

where $Y_{1a}^2 = y_{1ca}^2 + y_{1sa}^2$, $Y_{2a}^2 = y_{2ca}^2 + y_{2sa}^2$, $Z_{2a}^2 = z_{2ca}^2 + z_{2sa}^2$ represent the modal amplitudes and $C_{2a} = y_{2ca}z_{2ca} + y_{2sa}z_{2sa}$ represents cross terms.

2.3 Step 3 - Localised Stability

In the third step of the analysis we examine the first order differential equations (13) to assess the stability boundary of the semi-trivial solution. The external excitation will lead directly to in-plane motion. With increasing excitation amplitude either of the out-of-plane modes can be excited, marking the boundary of the semi-trivial solution parameter space. For excitation of either out-of-plane modes there must be localised instability about the zero amplitude response for that mode. To find the boundary of the semi-trivial solution in parameter space we therefore examine the localised stability of each out-of-plane mode about the zero point assuming that the other out-of-plane mode has zero averaged amplitude.

For the first out-of-plane mode we can write

$$\begin{Bmatrix} y_{1ca}^{'} \\ y_{1sa}^{'} \end{Bmatrix} = \epsilon \begin{bmatrix} -\xi_{y1}\omega_1 & -\dfrac{N_1\Delta}{4\omega_1} - \mu\omega_1 + \dfrac{W_{12}Z_{2a}^2}{4\omega_1} \\ -\dfrac{N_1\Delta}{4\omega_1} + \mu\omega_1 - \dfrac{W_{12}Z_{2a}^2}{4\omega_1} & -\xi_{y1}\omega_1 \end{bmatrix} \begin{Bmatrix} y_{1ca} \\ y_{1sa} \end{Bmatrix} \tag{14}$$

where we have set the second out-of-plane mode amplitudes to zero and neglected the higher order y_{1ca} and y_{1sa} terms as we are considering the stability about the $y_{1a} = 0$ point. The resulting eigenvalues, χ (where we apply the scaling $\chi \to \epsilon\chi$), are given by

$$16\omega_1^2\chi^2 + 32\xi_{y1}\omega_1^3\chi + W_{12}^2Z_{2a}^4 - 8W_{12}\mu\omega_1^2Z_{2a}^2 + 16\omega_1^4(\mu^2 + \xi_{y1}^2) - N_1^2\Delta^2 = 0 \tag{15}$$

We note that initially when the excitation amplitude is small (such that Δ and Z_{2a}^2 are small) the eigenvalues of the matrix have negative real parts and hence the stable solution set is from zero excitation up to the boundary at which the real part of one of the eigenvalues is zero. This stability boundary is given by:

$$W_{12}^2 Z_{2a}^4 - 8W_{12}\mu\omega_1^2 Z_{2a}^2 + 16\omega_1^4(\mu^2 + \xi_{y1}^2) - N_1^2\Delta^2 = 0 \tag{16}$$

Using the same technique for the second out-of-plane mode and noting that $\omega_2 = 2\omega_1$ and $W_{22} = 4W_{12}$, the local eigenvalue equation is given by

$$16\omega_1^2\chi^2 + 64\xi_{y2}\omega_1^3\chi + 3W_{12}^2 Z_{2a}^4 - 32W_{12}\mu\omega_1^2 Z_{2a}^2 + 64\omega_1^4(\mu^2 + \xi_{y2}^2) = 0 \tag{17}$$

As before, when the excitation amplitude is small the eigenvalues have negative real parts and hence the stable solution set is from zero excitation up to the boundary at which the real part of one of the eigenvalues is zero. When μ is negative the eigenvalues are stable for all Z. For positive μ the stability boundary is defined by

$$3W_{12}^2 Z_{2a}^4 - 32W_{12}\mu\omega_1^2 Z_{2a}^2 + 64\omega_1^4(\mu^2 + \xi_{y2}^2) = 0 \tag{18}$$

For this equation real positive solutions for Z_{2a}^2 only exist if $\mu \geq \sqrt{3}\xi_{y2}$, and if this condition is satisfied there are two real positive solutions for Z_{2a}^2 and hence two stability boundaries. For $\mu < \sqrt{3}\xi_{y2}$ the second out-of-plane mode is stable about the zero amplitude position for all Z_{2a} and hence for all excitation amplitudes Δ.

Finally to allow the calculation of the semi-trivial solution boundary we must derive an equation for Z_{2a} in terms of the excitation amplitude noting that just below a point on the solution boundary the out-of-plane modes are zero. We can therefore reduce the equations for the in-plane mode in equation (13) to

$$\begin{aligned} z_{2ca}^{'} &= -\tfrac{\epsilon}{\omega_2}\left(\xi_{z2}\omega_2^2 z_{2ca} + [\mu\omega_2^2 - \tfrac{3}{8}W_{22}Z_{2a}^2]z_{2sa}\right) \\ z_{2sa}^{'} &= \tfrac{\epsilon}{\omega_2}\left([\mu\omega_2^2 - \tfrac{3}{8}W_{22}Z_{2a}^2]z_{2ca} - \xi_{z2}\omega_2^2 z_{2sa} - \tfrac{1}{2}B\Delta\omega_2^2\right) \end{aligned} \tag{19}$$

Setting these equations to zero, the steady state amplitude of oscillation of the second in-plane mode may we written as:

$$16\omega_1^4 B^2\Delta^2 = 64\omega_1^4(\mu^2 + \xi_{z2}^2)Z_{2a}^2 - 48\omega_1^2\mu W_{12}Z_{2a}^4 + 9W_{12}^2 Z_{2a}^6 \tag{20}$$

Solving equation (20) with equation (16) and equation (18) allows the amplitude of excitation at which the boundary of stability occurs for the first and second out-of-plane modes respectively to be found as a function of the support motion frequency. We first express the semi-trivial solution boundary

equations, 16 and 18, and the amplitude equation 20 in nondimensional form using the parameters:

$$\begin{aligned} \epsilon_s &= \tfrac{\sigma_s}{E} \qquad \gamma_\theta = \rho g L \cos(\theta)\sigma_s \\ \hat{Z}_{2a} &= \tfrac{Z_{2a}}{L} \qquad\quad \hat{\Delta} = \tfrac{\Delta}{L} \end{aligned} \tag{21}$$

Using these expressions and the equations in (3), the first out-of-plane boundary equation 16 may be written as

$$\pi^4 \hat{Z}_{2a}^4 - 8\epsilon_s \mu \pi^2 \hat{Z}_{2a}^2 + 16\epsilon_s^2(\mu^2 + \xi_{y1}^2) - \frac{144}{(12+\lambda^2)^2}\sin^2(\theta)\hat{\Delta}^2 = 0 \tag{22}$$

and the second out-of-plane boundary equation (18) as

$$3\pi^4 \hat{Z}_{2a}^4 - 32\epsilon_s \mu \pi^2 \hat{Z}_{2a}^2 + 64\epsilon_s^2(\mu^2 + \xi_{y2}^2) = 0 \tag{23}$$

where Irvine's parameter may be written as $\lambda^2 = \gamma_\theta^2/\epsilon_s$. Finally the steady state amplitude of oscillation of the second in-plane mode equation (20) may we written as:

$$16\epsilon_s^2 \cos^2(\theta)\hat{\Delta}^2 = 64\pi^2\epsilon_s^2(\mu^2 + \xi_{2z}^2)\hat{Z}_{2a}^2 - 48\pi^4\epsilon_s\mu\hat{Z}_{2a}^4 + 9\pi^6\hat{Z}_{2a}^6 \tag{24}$$

(Note that when reversing the transforms $\xi_{y1} \rightarrow \epsilon\xi_{y1}$ etc the scaling term ϵ cancels out.)

3 Stability Boundaries: Theory, Simulation and Experiment

In this paper we consider a small scale, 1.98 m long, steel cable which is inclined at 20^o to the horizontal. The cable has a diameter of 0.8 mm and has a mass of 0.67 kg/m (in the experiments this is achieved by attaching lead weights at 60 mm interval). The static tension of the cable is 205 N. The experimental setup is shown in figure 2. This gives nondimensional parameter values: $\epsilon_s = 2.04 \times 10^{-3}$ and $\gamma_\theta = 13.08 \times 10^{-3}$.

MATLAB/Simulink was used in conjunction with a dSpace DS1104 RD controller board to implement an actuator controller and data acquisition system. The cable is dynamically tested by a electrically driven ball-screw actuator with an in line mounted synchronous servo motor controlled by a servo drive which applies a displacement to the cable anchorage point in the vertical direction. The instrumentation used consists of two load cell to measure the static tension and the dynamic force acting at the cable anchorage, one LVDT displacement transducer to be able to track and control the actuator movement and a digital incremental encoder used to control the initial inclination of the cable. A high speed vision system [10] was used to measure the cable motion at nine different points both in-plane and out-of-plane.

Natural frequencies were identified experimentally using free vibration tests. They agreed well with the theoretical values (equation (4)) and are summarised in table 1. From the experimental data the

modal damping ratios for the first two modes over the range of oscillation amplitude of interest was estimated to all be approximately $\xi = 0.2\%$.

Table 1: Modal properties

	ω_{y2} [Hz]	ω_{z1} [Hz]	ω_{z1} [Hz]	ω_{z2} [Hz]
Experimental	4.4031	8.7623	4.7180	8.7665
Theoretical	4.4050	8.8101	4.7134	8.8101

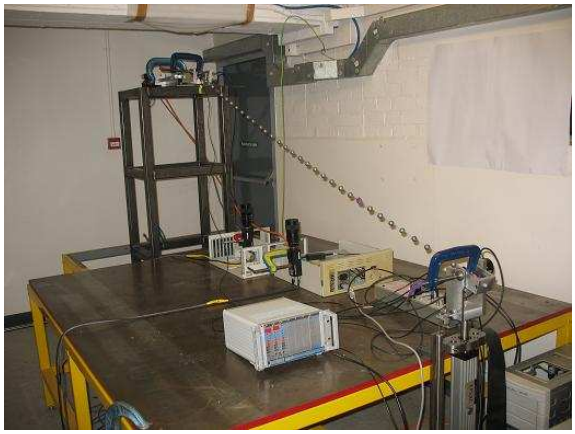

Figure 2: Experimental setup

3.1 Theoretical Stability Boundaries

The theoretical stability boundaries in terms of the normalised excitation amplitude Δ/L and normalised excitation frequency Ω/ω_2 are found by numerically solving equations (20) and (16) for the first out-of-plane mode and equations (20) and (18) for the second out-of-plane mode. The boundaries are shown in figure 3. For the first out-of-plane mode there is a single boundary, for excitation levels below this boundary the zero response of the out-of-plane mode is stable and above the zero response is unstable. For the second out-of-plane mode there are two stability boundaries for $\mu \geq \sqrt{3}\xi$. At low excitation levels, Δ the mode is stable about zero amplitude response, then with increasing Δ the lower boundary line is crossed and a second out-of-plane modal response is expected. If Δ is increased further so that the second boundary level is crossed the zero amplitude modal response becomes stable again.

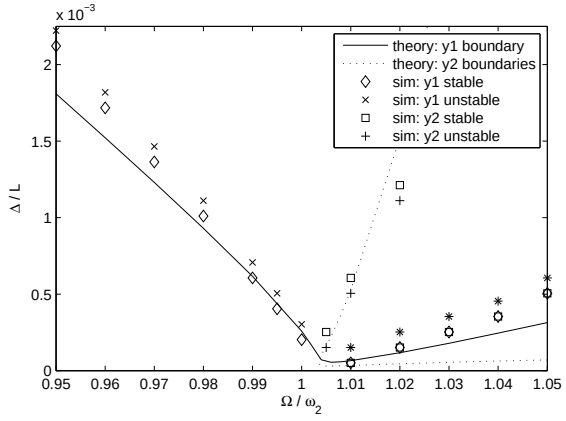

Figure 3: Stability boundaries: theoretical and simulation (with zero initial conditions) Note square crosses and diagonal crosses overlaid appear as stars.

3.2 Simulation Stability Boundaries

Simulation results were generated by using the matlab ode23s timestepping routine applied to equation (5). By inspection of equations (5), it can be seen that even when one of the out-of-plane modes is unstable about zero amplitude no modal response will occur unless there is an external disturbance. Therefore in the simulations the excitation is run for 25 s, by which time the directly excited second in-plane mode response is approximately steady state. At 25 s a disturbance, in the form of a 0.02 s pulse, is applied to the velocity of both the out-of-plane modes, and the stability of the modes is assessed. This is done for a range of excitation amplitudes with increments of 0.2 mm. As an example, figure 4 shows the mode response when the system is excited at a frequency of $\Omega/\omega_2 = 0.97$ for two amplitudes, 2.7 mm and 2.9 mm which correspond to stable and unstable y_1 mode response respectively (y_2 is stable for both cases).

Simulation of stability boundary results in which the initial conditions for the second in-plane mode are zero are shown in figure 3. For each value of Ω/ω_2 excitation amplitudes (with a resolution of 0.2 mm) either side of the observed modal stability boundaries are marked, for example for $\Omega/\omega_2 = 0.97$, considering the y_1 mode, 2.7 mm excitation is marked as stable and 2.9 mm as unstable. From this figure, for the first out-of-plane mode it can be seen that there is good agreement between the theory and the simulations for low negative μ values (such that $0.98 \leq \Omega/\omega_2 \leq 0$). If μ is more negative the agreement deteriorates. This is due to the scaling in which it was assumed that Δ was small. There is no instability in the second mode for negative μ values as indicated by the theory. For positive μ values there is good agreement for the upper second mode stability boundary (with the same deterioration at larger values of

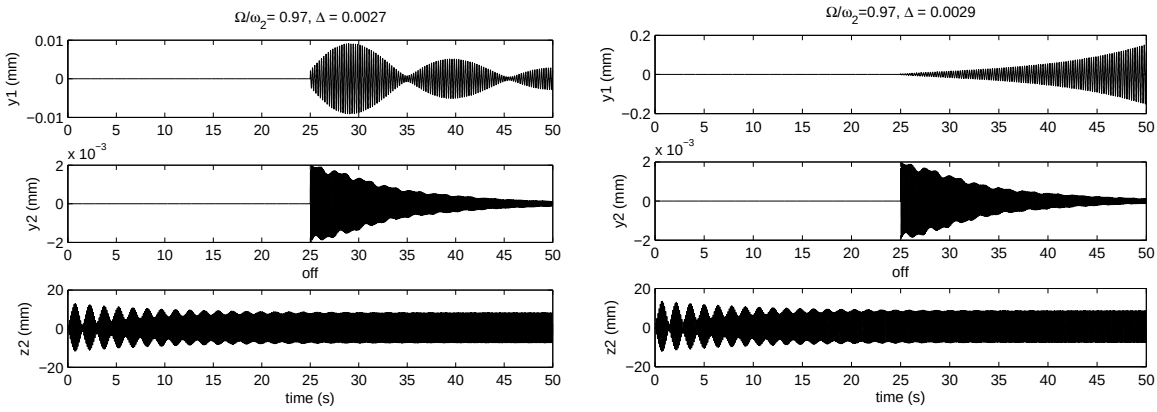

Figure 4: Simulation time responses, $\Omega/\omega_2 = 0.97$, with excitation amplitudes of 2.7 and 2.9 mm

Δ). However the simulations do not agree with the theory for the lower second mode and the first mode stability boundaries.

The reason for this disagreement is that the lower boundary does not correspond to to the zero initial condition case which is computed using the simulation. To see this, consider the equation for the amplitude of the second mode in-plane response (with zero response in the other modes), equation (20), which can be written

$$\frac{\mathrm{d}\Delta}{\mathrm{d}Z_{2a}} = \frac{Z_{2a}}{16\omega_1^4 B^2 \Delta}\left(64\omega_1^4(\mu^2+\xi_{z2}^2) - 96\omega_1^2\mu W_{12}Z_{2a}^2 + 27W_{12}^2Z_{2a}^4\right) \tag{25}$$

There are positive real values of Z_{2a} that satisfy $\mathrm{d}\Delta/\mathrm{d}Z_{2a} = 0$ if $\mu \geq \sqrt{3}\xi_{z2}$. This indicates that there are multiple solutions for Z_{2a} for a given Δ for $\mu \geq \sqrt{3}\xi_{z2}$ i.e. the curve has a fold. Using equation (20), an example relationship between Δ and Z_{2a} is shown in figure 5 for the case where $\mu = 0.03$. The points at which the out-of-plane modes become unstable are indicated on the curve. The region of the curve represented by the dashed line is unstable. This may be shown by rewriting equation 19 in matrix form:

$$\mathbf{Z}_{v2a}^{'} = f(\mathbf{Z}_{v2a}) \simeq f(\bar{\mathbf{Z}}_{v2a}) + (\mathbf{Z}_{v2a} - \bar{\mathbf{Z}}_{v2a})Df(\hat{\mathbf{Z}}_{v2a}) \tag{26}$$

where $\mathbf{Z}_{v2a} = \{z_{2ca}\ ,\ z_{2sa}\}^T$ and $Df(x)$ is the Jacobian of $f(x)$. The stability of the response is governed by the eigenvalues of the Jacobian evaluated at the possible equilibrium points, $\bar{\mathbf{Z}}_{v2a}$, such that $f(\bar{\mathbf{Z}}_{v2a}) = 0$, ie along the line governed by (20). For simulations with zero initial conditions, in the hysteretic region, where there are two stable solutions for the amplitude of the second in-plane response, the simulation is always attracted to the low amplitude solution. Therefore instability in the out-of-plane modes only occurs when the excitation amplitude Δ exceeds the lower saddle-node bifurcation (point A

in Figure 5), at which point the amplitude of second in-plane mode jumps to the larger solution curve, point D in Figure 5. This higher solution is beyond the instability points of the two out-of-plane modes (i.e. point D is to the right of points B and C in Figure 5) so both modes go unstable at the jump from the lower bifurcation point (i.e. A to D in Figure 5). From equation (25) the saddle-node bifurcation (point A) occurs when:

$$Z_{2a}^2 = \frac{8\omega_1^2\mu}{9W_{12}}\left(2 - \sqrt{1 - 3\left(\frac{\xi_{z2}}{\mu}\right)^2}\right) \tag{27}$$

Figure 6 shows the turning point in terms of Δ (using equation 20 and 27) compared with the simulation data assuming zero initial conditions, it can be seen that there is reasonably good agreement.

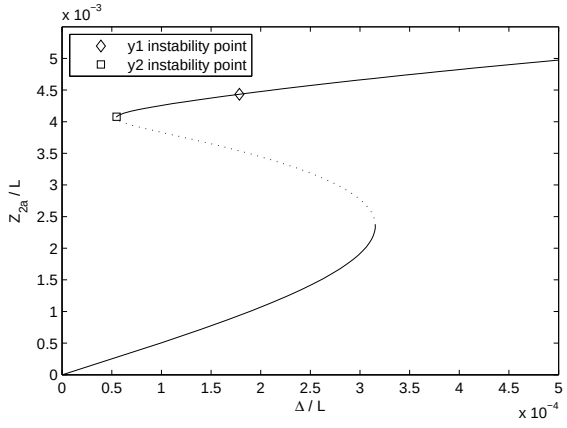

Figure 5: Response of the second in-plane mode (assuming other modes remain stable) when excited at frequency $\Omega/\omega_2 = 1.03$ and amplitude Δ

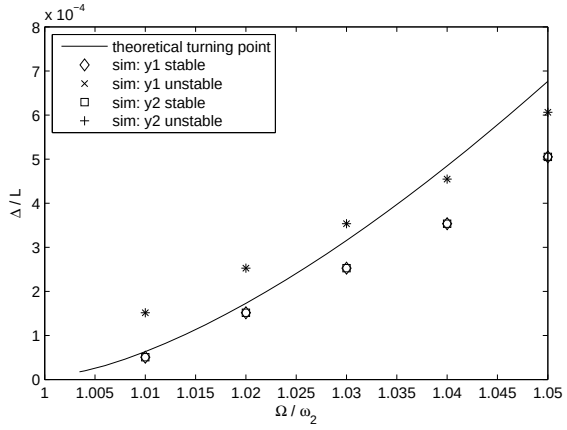

Figure 6: Simulation stability points for positive μ compared with the turning point (equation 27)

To simulate the theoretical instability boundary which exists a point B in Figure 5, the system must oscillate at the larger Z_{2a} amplitude solution before the out-of-plane disturbance is applied. This was achieved in the numerical simulation by initially setting an excitation amplitude higher than the turning point value and reducing it to the desired level after 15s. After 25s a pulse disturbance was applied to the out-of-plane modes to test for modal instability about the zero response position. The simulation results are shown in figure **??**. It can be seen that there is excellent agreement with the theoretical predictions.

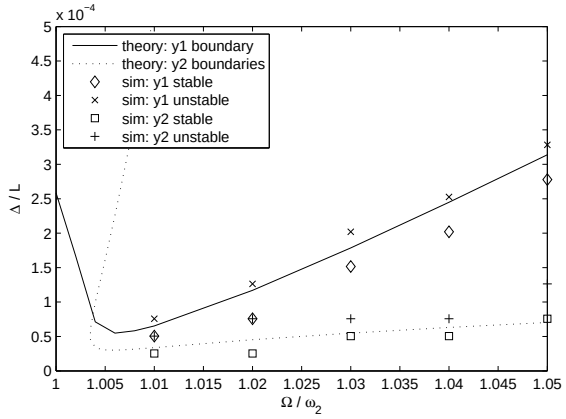

Figure 7: Simulation stability points for positive μ when the second in-plane response is at the higher amplitude solution

3.3 Experimental Stability Boundaries

In the experimental tests it was found that a small amount of oscillation (around 1 mm amplitude) of the second out-of-plane mode was present throughout all tests. Growth in amplitude of this mode was not observed to take place before instability of the first out-of-plane mode. The system was allowed 400 periods of external excitation for the transient response to decay. After the 400 periods a disturbance was introduced, in the form of a slight impulse applied horizontally to the mid-span lead weight. The out-of-plane amplitude of oscillation was then monitored for a further 400 periods to ascertain the stability of the mode. This procedure was repeated for increasing amplitudes of excitation up to the instability point for a range of forcing frequencies up to $\Omega/\omega_2 < 1.04$.

Figure 8 shows the experimental stability points, which also show very good agreement with the theoretical boundary for $\mu < 0.02$. Above $\mu = 0.02$ the results diverge from the theoretical stability values, as with the simulations this is because the initial conditions are zero and so the modal instability only occurs after the excitation amplitude exceeds the turning point defined by equation (27). It can be seen that this relationship agrees well with the experimental results for $\mu > 0.02$.

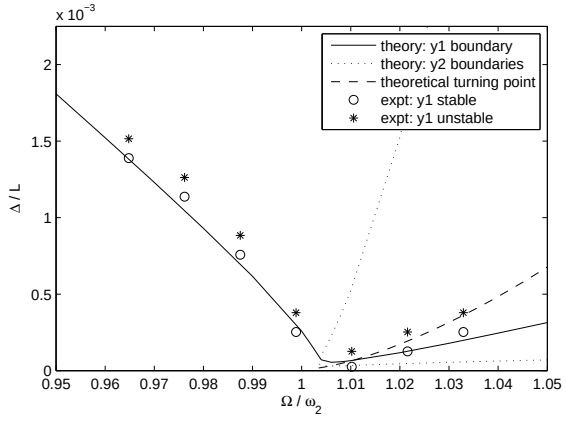

Figure 8: Theoretical and experimental stability boundaries

3.4 Discussion

The simulation and experimental observations give very goof agreement well with the new theoretical model. We have demonstrated how t he out-of-plane modes can go unstable at the theoretical stability boundaries defined by equations (16) and (19) for the first out-of-plane mode and by equations (18) and (19) for the second out-of-plane mode. The nondimensional equivalent to these equations are equations (22) and (24) and equations (23) and (24) respectively. However when $\mu \geq \sqrt{3}\xi_{z2}$ there are two solutions for Z_{2a} in the hysteretic region. This fold in the relationship between Z_{2a} and Δ can have the effect of raising the excitation level required for the onset of vibrations in the out-of-plane modes as the instability occurs on the larger Z_{2a} branch (see figure 5 for the case where $\mu = 0.03$). If for example the cable is initially considered to have zero initial conditions then the excitation level must exceed the first turning point, defined by equation (27), in the relationship between Z_{2a} and Δ before the larger Z_{2a} branch is reached. If this turning point occurs at a larger Δ than the instability point of either of the out-of-plane modes then out-of-plane oscillations in that mode are only observed at Δ values exceeding the turning point. For the cable considered in section 3, the resulting instability boundaries are shown in figure 8. The dotted line indicates the turning point which can lift the stability boundary depending on the initial conditions. We note that in the region where the turning point is below the theoretical stability boundaries, the turning point relationship does not effect the Δ required for instability of the semi-trivial solution – the theoretical stability boundaries are conservative.

4 Parametric Study of Stability Boundaries

The most widely used stabilities curves when studying resonance 2:1 are the ones presented in [2] and are used in practical bridge design recommendations, such as that produces by Setra [15], to provide guidance as to whether the expected cable anchorage motions would be large enough to initiate parametric excitation. The equations of the stability boundary in both works is found by studying a linear one-degree-of-freedom Mathieu-Hill type equation. Since they reduce the study to a single degree of freedom they calculate y_1 and y_2 boundaries separately, the first in 2:1 resonance, the second excited in 1:1 resonance. We start comparing y_1 stability regions. Eq 28 shows the stability boundary given by [2], Eq 30 shows the one given in the Setra manual [15] for 2:1 resonance.

$$\hat{\Delta} = 2\frac{\sigma_s}{Esin(\theta)}\sqrt{\left[\frac{\Omega}{2\omega_1}^2 - 1\right]^2 + \left[2\xi_n\frac{\Omega}{\omega_1}\right]^2} \tag{28}$$

$$\hat{\Delta} = 2\frac{\sigma_s}{Esin(\theta)}\sqrt{\left[\frac{\Omega}{2\omega_1}^2 - 1\right]^2 + 4\xi_n^2} \tag{29}$$

The resulting boundary regions plot is almost identical, in both cases, the minimum amplitude at which parametric resonance occurs is $\hat{\Delta} = \frac{4\xi\epsilon_s}{sin(\theta)}$ when $\Omega/2\omega_1 = 1$, i.e, $\mu = 0$. We now compare our results with the boundary proposed in [15].

In figure 9 comparison between our analytical model and [15] is shown. The minimum amplitude the minimum amplitude for which parametric resonance occurs is $\hat{\Delta} = \frac{4\xi\epsilon_s}{sin(\theta)}$ for both models, but while [15] predicts it to occur at $\Omega/2\omega_1 = 1$, averaging predicts this minimum to be shifted to a slightly higher frequency. This shifting of the minimum and the reduction in amplitude of the higher frequency sides of the stability boundary are a direct consequence of the hardening that cables suffer due to the geometric cubic nonlinearity. This nonlinearity is not taken into account in previous stability models, such as [2,15], and as a result the match with experimental data (as shown in the previous section) will be reduced. The reduction in amplitude of the curve shows clearly that parametric resonance can occur for much smaller values that previously predicted [2, 15] when $\Omega/2\omega_1 > 1$.

By substituting $\hat{\Delta} = \frac{4\xi\epsilon_s}{sin(\theta)}$ into equations (22) and (24) we can obtain the following cubic equation to calculate the shifting of the minimum of the stability curve.

$$\mu^3 + 7Q\xi\mu^2 + \left[\xi^2 - 15Q^2\xi^2\right]\mu + \left[9Q^3\xi^3 + 4Q\xi^2 - \frac{4\epsilon_s\xi^2}{tan^2(\theta)}\right] = 0 \tag{30}$$

where $Q = \frac{12}{12+\lambda^2}$. Figure 10 shows how the values of μ evolve as the non dimensional system parameters are changed. Figure 11 shows how the stability regions change their shape for different groups of cable

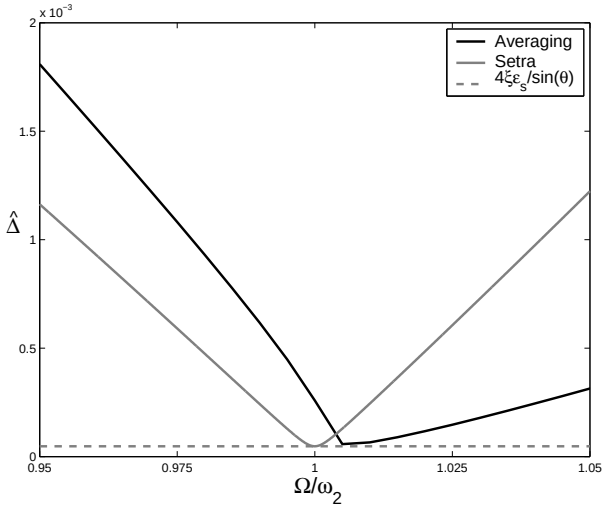

Figure 9: Setra recommendations [15] stability boundary and proposed stability boundaries

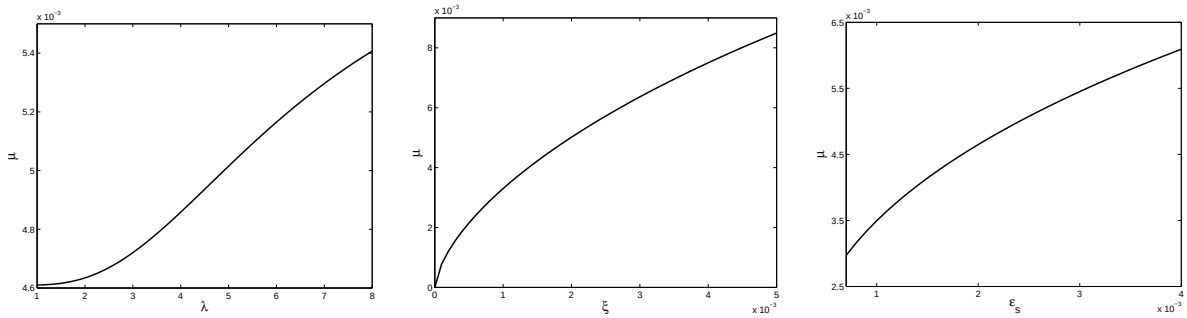

Figure 10: Shifting of the minimum versus cable nondimensional parameters.

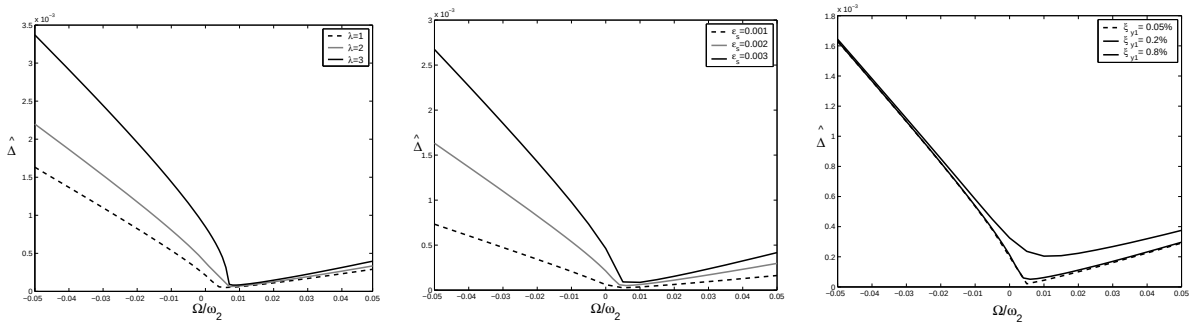

Figure 11: Stability regions for different cable nondimensional parameters.

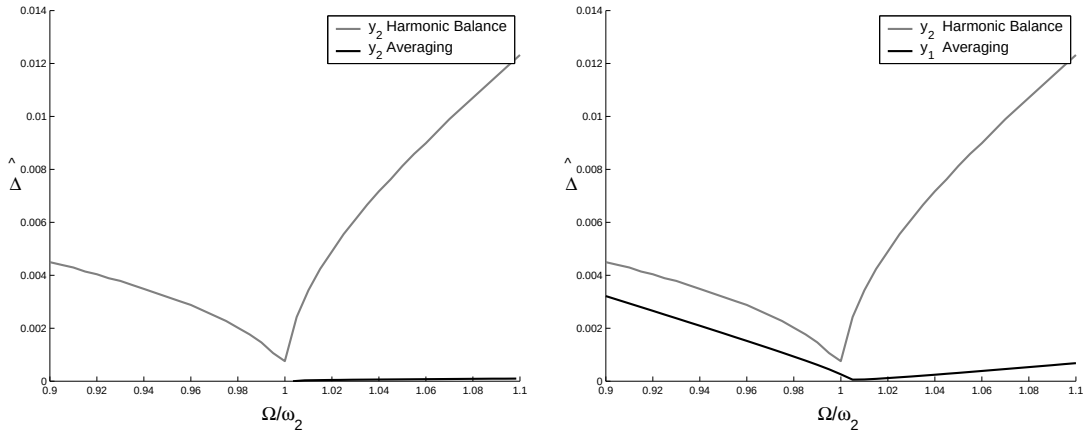

Figure 12: Stability regions for different cable nondimensional parameters.

nondimensional parameters.

Neither [2] nor [15] give a explicit equation to calculate the y_2 stability region. It is commonly assumed than resonance 1:1 is not likely to appear since the values of forcing amplitude necessary for it to occur are very high. That will only be the case if we reduce the problem to a SDOF case. We can solve the stability problem by applying Harmonic Balance Method (for the 1:1 resonance, we can not apply first order averaging, even second order averaging gives only zero since is eliminated as a lower order resonance, for most systems resonance 1:1 is a rather trivial case). Redefining our problem as SDOF, the y_2 stability boundary can be calculated by applying the Harmonic Balance Method to equation.

$$\ddot{y_2} + h_2 \dot{y_2} + \left(\omega_2^2 + N_2 \delta\right) y_2 = 0 \tag{31}$$

Following the approach considered in [5] we solve the problem in the eigenvalue form. Taking three terms of the Fourier expansion one obtains an non-symmetric 14x14 matrix. If the subtraction of any eigenvalue from the damping constant leaves a positive real part, the corresponding trivial solution is unbounded and the solution is unstable. See [5] for more information.

Figure 12(a) shows comparison between the y_2 stability boundary calculated with a SDOF model and applying the harmonic balance method with the three mode model we proposed in this work, i.e. 3DOF using averaging methods. The curve corresponding to the SDOF model is much higher that the one calculated by the 3DOF — so much so that they cannot easily be plotted at the same scale, Figure 12(a). For frequencies above resonance $\mu > 0$the modal interaction is clearly a more important effect that 1:1 resonance. For values $\mu < 0$ the 1:1 resonance can desestabilize the y_2 mode (modal interaction

can not for this range of values) but the amplitude threshold is high (higher than the for y_1 in the same range of values), see Figure 12(b).

Conclusions

In this paper we have presented an extended three mode modal for the vibration of an inclined cable with harmonic support excitation at the lower end of the cable. By including the model coupling terms, and using averaging, the three mode model has been used to explain some subtle dynamic behaviour which occurs around the 2:1 internal resonance of the in and out-of-plane modes. In particular the effect of the hysteretic jump on the numerical and experimental tracking of the lower stability branch for y_2 solutions has been explained in detail.

As part of this study as series of experimental tests were carried out using a scaled inclined cable with an actuator to give vertical excitation input at the lower support. Tests were carried out to observe the onset of oscillations in the out-of-plane modes, and these were compared with analysis and simulation from the three mode model. Close agreement was found between the experimental and numerical results, giving a high degree of confidence in the extended three mode model. This also demonstrates the importance of including the nonlinear coupling terms when studying the stability boundaries close to the 2:1 resonance region. Currently these coupling effects are not usually considered, but the results from this study show that the onset of oscillations in the out-of-plane modes can occur at lower amplitudes of excitation than predicted by previous models without coupling.

Acknowledgments

The authors would like to acknowledge the support of the EPSRC: Alicia Gonzalez-Buelga is supported by EPSRC grant (GR/S49780) and David Wagg via an Advanced Research Fellowship.

References

[1] A.H. Nayfeh and P.F. Pai. *Linear and Nonlinear Structural Mechanics*. John Wiley, 2004.

[2] J.L. Lilien and A. Pinto da Costa. Vibration amplitudes caused by paramteric excitation of cable-stayed structures. *Journal of Sound and Vibration*, 174(1):69–90, 1994.

[3] H.M. Irvine. *Cable structures*. MIT Press, Cambridge, MA, 1981.

[4] W. Szemplinska-Stupnicka. The generalized harmonic balance method for determining the combinations resonance in the parametric dynamic systems. *Journal of Sound and Vibration*, 58:347–361, 1978.

[5] K. Takahashi. An approach to investigate the instablity of the multiple-degree-of-freedom parametric dynamic systems. *Journal of Sound and Vibration*, 78(4):519–529, 1981.

[6] K. Takahashi. Dynamic stability of cables subjected to an axial periodic load. *Journal of Sound and Vibration*, 144(2):323–330, 1991.

[7] F. Benedettini, G. Rega, and R. Alaggio. Non-linear oscillations of a nonlinear model of a suspended cable. *Journal of Sound and Vibration*, 182:775–798, 1995.

[8] N.C. Perkins. Modal interactions in the non-linear response of elastic cables under parametric/external excitation. *Internacional Journal Non-linear Mechanics*, 27(2):233–250, 1992.

[9] V.N. Pilipchuk and R.A. Ibrahim. Nonlinear modal interactions in shallow suspended cables. *Journal of Sound and Vibration*, 227(1):1–28, 1999.

[10] J.H.G. Macdonald, C.A. Taylor, B.T. Thomas, and E.L. Dagless. Ream time remote monitoring of dynamic displacements by computer vision. In *6th Soc. for Earthquake and Civil Eng. Dynamics Conf.*, pages 389–396, 1998.

[11] Y. Warmitchai, T. Fujino, and A. Susumpov. A nonlinear dynamic model for cables and its application to a cable structure-system. *Journal of Sound and Vibration*, 187(3):695–712, 1995.

[12] A. Tondl, T. Ruijgrok, F. Verhulst, and R. Nabergoj. *Autoparametric Resonance in Mechanical Systems*. Cambridge, 2000.

[13] F. Verhulst. *Nonlinear Differential Equations and Dynamical Systems*. Springer, 1996.

[14] T. Bakri, R. Nabergoj, A. Tonel, and F. Verhulst. Parametric excitation in non-linear dynamics. *Internacional Journal Non-linear Mechanics*, 39:311–329, 2004.

[15] Setra. *Cable Stays, Recommendations of French interministerial commission on Prestressing*. Center des Techniques des Ouvraes d'Art, Bagneux Cedex, France, 2002.